

Masked GANs for Unsupervised Depth and Pose Prediction with Scale Consistency

Chaoqiang Zhao, Gary G. Yen, *Fellow, IEEE*, Qiyu Sun, Chongzhen Zhang, Yang Tang, *Senior Member, IEEE*

Abstract—Previous works have shown that adversarial learning can be used for unsupervised monocular depth and visual odometry (VO) estimation. However, the performance of pose and depth networks is limited by occlusions and visual field changes. Because of the incomplete correspondence of visual information between frames caused by motion, target images cannot be synthesized completely from source images via view reconstruction and bilinear interpolation. The reconstruction loss based on the difference between synthesized and real target images will be affected by the incomplete reconstruction. Besides, the data distribution of unreconstructed regions will be learned and help the discriminator distinguish between real and fake images, thereby causing the case that the generator may fail to compete with the discriminator. Therefore, a MaskNet is designed in this paper to predict these regions and reduce their impacts on the reconstruction loss and adversarial loss. The impact of unreconstructed regions on discriminator is tackled by proposing a boolean mask scheme, as shown in Fig. 1. Furthermore, we consider the scale consistency of our pose network by utilizing a new scale-consistency loss, therefore our pose network is capable of providing the full camera trajectory over the long monocular sequence. Extensive experiments on KITTI dataset show that each component proposed in this paper contributes to the performance, and both of our depth and trajectory prediction achieve competitive performance.

Index Terms—Adversarial learning, unsupervised learning, depth estimation, visual odometry, boolean mask, scale consistency

I. INTRODUCTION

Understanding the 3D structure of the scene and estimating the ego-motion are two basic tasks of autonomous robots. With the development in deep learning (DL) technology, DL-based depth and pose prediction have achieved outstanding results in both supervised [1], [2] and unsupervised manners [3], [4]. Because of free from expensive ground truth during training, unsupervised methods have been widely studied [5], [6], in which depth and pose networks are jointly trained on the monocular videos. Meanwhile, the geometric constraint (view reconstruction loss) based on the output of networks is regarded as the supervised signal. To improve the the

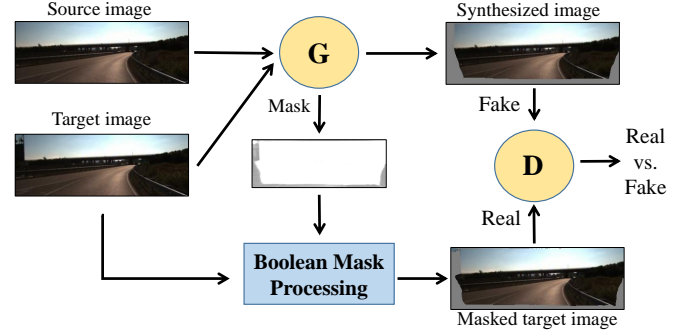


Fig. 1. Architecture overview. Our unsupervised adversarial learning framework consists of two major components, generator (G) and discriminator (D). Adjacent frames are taken to G to reconstruct target image and predict a mask of unreconstructed regions. Instead of sending the target image to discriminator directly, a “boolean mask processing” step is designed to preprocess it. As shown in the “masked target image”, the unreconstructed regions similar to synthesized image are created, thereby reducing the effect of unreconstructed regions on discriminator.

performance of depth estimation, recent works also combine the mask [3], semantic segmentation [7], [8] or optical flow [9], [10] prediction networks for multi-tasks training framework. The intrinsic relationships among the above tasks are used as additional constraints during training, thereby further improving the performance of networks. Compared with the traditional visual odometry (VO) or structure from motion (SfM) methods [11]–[14] that rely heavily on the strong back-end optimization process [15], DL-based methods can estimate the 6-DOF (degrees of freedom) ego-motion and pixel-level dense depth maps in an end-to-end manner. Furthermore, with the ability of high-level robust feature extraction, DL-based methods can adapt well to the scenarios where traditional methods do not perform well, such as high dynamic range (HDR) or low texture environments.

Adversarial learning shows strong capabilities in the field of image processing recently [16]. Recent works [17]–[24] have demonstrated that introducing the adversarial learning for depth and pose estimation can significantly improve the accuracy of these two tasks. In [17], [20], [25], adversarial learning is combined with the framework of unsupervised methods for depth and pose estimation based on monocular videos. During training, the images reconstructed by view reconstruction and the real images are taken into the discriminator to learn different distributions of these images. Meanwhile, the purpose of generator is to reconstruct images that are highly similar to the target images by improving depth and pose estimation. The adversarial learning process

This work was supported by the National Key Research and Development Program of China under Grant 2018YFC0809302, the National Natural Science Foundation of China under Grant Nos. 61751305, 61673176, by the Programme of Introducing Talents of Discipline to Universities (the 111 Project) under Grant B17017. (Corresponding author: Yang Tang.)

C. Zhao, Q. Sun, C. Zhang and Y. Tang are with the Key Laboratory of Advanced Control and Optimization for Chemical Process, Ministry of Education, East China University of Science and Technology, Shanghai, 200237, China (e-mail: yangtang@ecust.edu.cn (Y. Tang)).

Gary G. Yen is with the School of Electrical and Computer Engineering, Oklahoma State University, Stillwater, OK 74075 USA (e-mail: gyen@okstate.edu).

prompts the generator to produce a higher quality of depth and ego-motion estimation. In addition, to assist the generator to train well and compete against the discriminator, the same traditional reconstruction loss function as documented in [3] is used to reduce the differences between synthetic and real images. However, in [17], [20], [25], since the visual field changes between target and source images, edge regions of synthesized images cannot be reconstructed well by view construction and bilinear interpolation, as shown in Fig. 2. The unreconstructed regions are inevitable and will not be removed by the training of generator. If these inevitable distinguishing features are learned by the discriminator, the generator will be at a disadvantageous status in adversarial learning, which is overlooked by previous works [17], [20], [25]. Hence, the performance of the generator (depth and pose networks) will be heavily affected. In this paper, we focus on this problem and tackle this challenge by proposing a boolean mask processing step, as shown in Fig. 1.

In addition, previous unsupervised methods, such as [3], [9], [10], [20], are trained by monocular frame snippets. There is lack of a suitable loss function to constrain the scale consistency of predicted results among different snippets, i.e., the scale factors of the poses and depth maps predicted by networks in two adjacent snippets are different. As a result, because of the scale-inconsistency among different image snippets, the global trajectory of monocular videos cannot be provided by pose network, and the scale-inconsistent depth maps cannot be used in practice. In order to have a scale consistent estimation of pose network, Bian *et al.* [26] consider this challenge and propose a geometry consistency loss. Different from [26], we utilize the structural similarity (SSIM) algorithm [27] to further constrain the structural similarity and scale-consistency between adjacent snippets.

In this paper, we consider the inherent differences between synthesized and target images, and propose a boolean mask processing to eliminate the influence of the unreconstructed regions on adversarial learning. A MaskNet is designed to estimate the regions on synthesized images that cannot be reconstructed, and we transfer the mask predicted by MaskNet to the boolean one, where 0, 1 respectively represent the unreconstructed and reconstructed pixels. Afterwards, before being sent to discriminator, real images are preprocessed by the step of boolean mask processing to generate similar unreconstructed regions as synthesized images. Therefore, the generator is assisted by boolean mask processing to compete against the discriminator. Besides, the mask predicted by MaskNet is also used to reduce the effects of dynamic objects and occlusions on the view reconstruction loss. A novel adaptive loss function based on SSIM is also designed in this paper to strengthen the scale consistency, and as a result our pose network has the ability to provide accurate trajectory over long monocular videos.

In summary, our main contributions are as follows: i) We introduce a masked GAN framework for pose and depth estimation, where the effects of occlusion and visual field changes on view reconstruction and adversarial learning are considered. ii) This paper discusses the effect of unreconstructed regions on adversarial learning, which is an issue

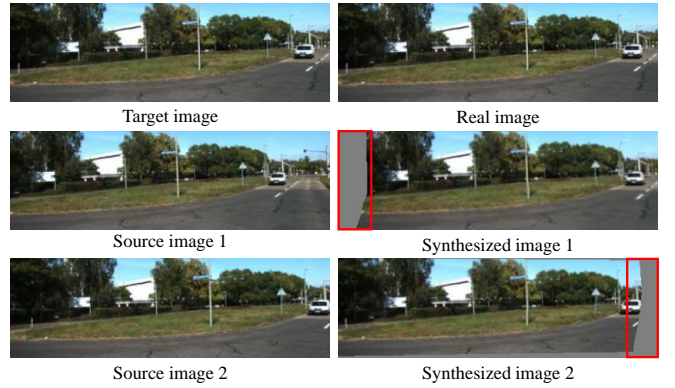


Fig. 2. Comparison of the real target image and the synthesized images. The synthesized target images (synthesized images 1 and 2) are synthesized from corresponding source images (source images 1 and 2) by view reconstruction algorithm. Due to the motion, the visual field changes between adjacent images, which causes the incomplete pixel correspondence between the target and source images. Therefore, edge regions in synthesized images cannot be synthesized from the source images because of the information miss caused by visual field changes.

ignored in previous works, and a boolean mask processing is proposed to eliminate this negative influence. iii) We consider the scale-inconsistent problem and propose a novel adaptive constraint for a better global trajectory prediction. Meanwhile, both the pose and depth networks proposed in this paper show competitive results on KITTI dataset [28].

In this paper, the previous works on monocular ego-motion and depth prediction are discussed in Section II. Section III introduces the proposed unsupervised masked GAN framework in detail. Section IV shows our experimental results of the proposed method on KITTI. Finally, this study is concluded in Section V.

II. RELATED WORK

Traditional 3D structure recovery is based on triangulation algorithm [14], which needs to find a set of matching pixels between multiple frames. With the technological advancements in DL, convolutional neural networks (CNNs) have shown their superb ability in monocular depth estimation. In this section, we review the previous works on DL-based monocular depth and ego-motion estimation.

Learning from the ground truth. Eigen *et al.* [1] introduce CNNs into monocular depth estimation and predict the depth in an end-to-end manner. Alex *et al.* [29] design a PoseNet based on CNNs for 6-DOF pose regression. Recently, in [30], [31], recurrent neural networks are also adopted to extract temporal features and preserve accumulated information to improve the estimation accuracy. Although the above methods [30], [31] achieve satisfactory accuracy in pose and depth estimation, both of them rely on the ground truth as the supervision signal, and the ground truth is difficult and expensive to acquire.

Recently, unsupervised monocular depth and ego-motion estimation has been well investigated because of freeing from the ground truth. According to the training manners, unsupervised learning methods can be divided into two types, learning from

stereo image pairs [32]–[34], and learning from monocular videos [3], [9], [35]. Although the training process of these methods depends on the geometric constraint between multi-frames, the trained networks can predict depth maps from a single image independently during testing.

Learning from stereo image pairs. Garg *et al.* [32] prove that the depth network can be trained by stereo image pairs in an unsupervised manner. They utilize the inverse depth prediction and the geometry between the stereo image pairs to reconstruct (inverse warping) the left image from the right image. The difference between synthesized and real images is used as a supervision signal during training. Godard *et al.* [33] follow and expand this idea by using a left-right consistency constraint to achieve better performance. Besides, in [34], [36], they introduce the pose estimation into the framework, and the networks are jointly trained on stereo sequences. The geometric constraints of the temporal (image sequences) and spatial (stereo image pairs) are utilized to improve the performance of ego-motion and depth estimation. Although the above methods [34], [36] can estimate the pose and depth with scale information, the accuracy relies heavily on the accurate calibration between stereo cameras.

Learning from monocular videos. Considering the advantages of a single camera system, such as small size and low power consumption, the unsupervised methods based on the monocular sequences are proposed to train the ego-motion and depth prediction networks. Zhou *et al.* [3] propose a framework that the depth network is jointly trained with the pose network by using monocular videos. They reconstruct the current image from its adjacent frames by view reconstruction, which relies on the output of pose and depth networks. Then, the reconstruction loss between reconstructed and raw images is computed as supervision signals. Afterwards, several researches follow [8]–[10], [37] and extend Zhou *et al.* [3] into multiple tasks, and the intrinsic geometric constraints among different tasks are utilized to strengthen the supervised signal and improve the training process. For example, Ranjan *et al.* [10] couple four fundamental problems (depth prediction, ego-motion estimation, optical flow and motion segmentation) through geometry constraints. Besides, a competitive training approach is proposed to balance the training process of each network. Various sensor data [38]–[40] are also used for depth and pose estimation. Nevertheless, due to the lack of appropriate scale consistent constraints, the pose network trained by unlabelled frame snippets cannot generate the full trajectory of a long video sequence. Therefore, Bian *et al.* [26] tackle this challenge by a geometry loss for scale consistency.

Learning with generative adversarial networks (GANs). Because of the outstanding performance of GANs on image processing, introducing adversarial learning into monocular depth estimation is becoming a hot topic. In the adversarial learning framework [41], a generator is designed to learn and mimic the distribution of real data, and a discriminator is designed to assess the quality of generated data and promote the performance of generator. Kumar *et al.* [17] apply GANs to monocular depth estimation. Their generator consists of depth and pose networks, and the output of networks are used to reconstruct images by view construction. Meanwhile,

a discriminator is designed to distinguish synthesized and real images. Recently, Almalioglu *et al.* [20] combine a recurrent learning approach with GAN for pose and depth estimation in an unsupervised manner. They leverage long short-term memory module (LSTM) to extract temporal information for pose estimation. Meanwhile, their generator estimates the depth map from a random vector z , i.e., the depth network cannot predict the depth map from a single image in an end-to-end manner. The most similar work to this paper is proposed in [25]. Li *et al.* introduce a mask network to reduce the effects of dynamic objects and occlusions on reconstruction loss, and a LSTM module is used for depth estimation. They also consider the geometric consistency of pose estimation. However, their depth network takes one single image and sequence information extracted by LSTM as input for depth estimation, i.e., their depth network can only be used on monocular sequences and cannot estimate the depth map from a single image, which is different from the proposed depth network herein. Besides, the constraint of geometric consistency in [25] is different from ours in the sense of expression.

Moreover, the above GAN-based methods [17], [20], [25] ignore the influence of occlusions and the visual field changes between adjacent frames on adversarial learning. The pixels between target and source images do not correspond exactly because of the visual field changes caused by motion, so that target images cannot be reconstructed completely from source images by view reconstruction algorithms and bilinear interpolation, as shown in Fig. 2. Therefore, the data distribution of unreconstructed regions in synthesized images is unique and cannot be eliminated exactly by the training of the generator. These unique distributions will be learned by discriminator, which will affect the adversarial learning process and the performance of generator, as shown in the experiments.

In this paper, we present a novel loss function to constrain the scale-consistency of our pose and depth networks. Meanwhile, considering the influence of unreconstructed regions on discriminator overlooked by previous works, we design a mask network to estimate these regions and introduce a boolean mask processing to eliminate their influence.

III. METHODOLOGY

In this section, we will give a brief introduction to the network architecture proposed in this paper, the self-supervised training framework, and the overall supervised signals.

A. Architecture overview

The framework of our unsupervised network is shown in Fig. 3. The generator takes a short frame snippet that consists of target image I_t and source image I_s , and the output of generator contains a depth map, a 6-DOF pose, and the boolean mask M_b corresponding to the unreconstructed region in synthesized images. Because of the inconsistent visual information between frames caused by view-field changes, synthesized images (fake images) produced by generator are incomplete. These unreconstructed areas in synthesized images become a distinctive feature between the real and fake images,

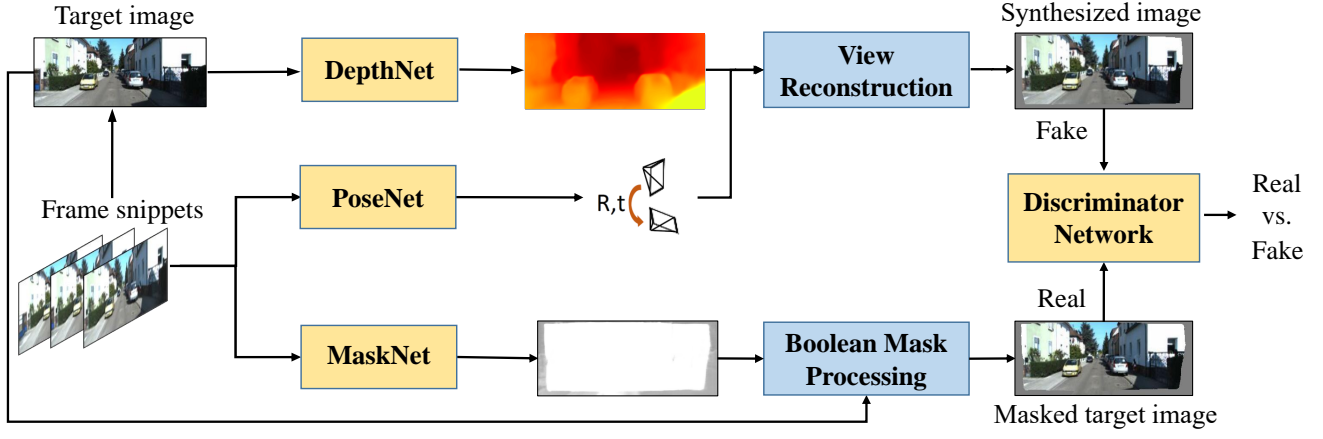


Fig. 3. Our unsupervised framework consists of two major parts, a generator and a discriminator. **Generator:** The main task of the generator is to reconstruct an image with the same data distribution as the target image by using the results of PoseNet and DepthNet. Due to the factors such as occlusions and changes in the visual field, some regions cannot be reconstructed (shown in the synthesized image), which will help the discriminator distinguish between real and fake images. Therefore, a MaskNet is designed to estimate these regions. We coupled our MaskNet with PoseNet for fewer parameters and easier training, which is similar to [3]. In order to show our full architecture clearly, we draw the PoseNet and MaskNet separately here. **Discriminator:** Before sending the real and synthesized target images to discriminator, we redesign the floating-point mask predicted by MaskNet into the boolean one, and the real target image is processed by the boolean mask. Hence, the major difference between real and fake images is removed, and this will make the discriminator learn a deeper feature and data distribution.

which will help the discriminator to distinguish them, thereby breaking the balance of the max-min game in adversarial learning. Moreover, because the field of view changes between adjacent frames is inevitable, these distinctive features (unreconstructed regions) usually persist and cannot be eliminated by continuous training of the generator. In this paper, to eliminate the effect of unreconstructed regions on the discriminator, we present a boolean mask to preprocess the real image and construct the same empty regions as the fake image. Therefore, the synthesized and target images contain the same data distribution of unreconstructed regions, which will have a positive effect on the adversarial learning and the training of the generator.

B. Unsupervised depth and pose estimation

Generator: Our generator consists of three networks for different tasks, as shown in Fig. 3, a DepthNet for single frame depth prediction, a PoseNet for ego-motion regression and a MaskNet for mask estimation. The view reconstruction algorithm is utilized to reconstruct the target image from a source image based on the output of pose and depth networks. The mask predicted by the MaskNet is utilized to eliminate the impacts of incomplete reconstruction changes on reconstruction loss and adversarial loss. For reconstruction loss, the effectiveness of mask has been demonstrated in recent works [3], [25]. For adversarial loss, we tackle this challenge by converting the mask into the boolean one to preprocess target images and construct the empty regions. We train the proposed architecture in the unsupervised manner, and the overall objective loss function is formulated as follows:

$$\mathcal{L}_g = \alpha \mathcal{L}_{basic} + \varphi \mathcal{L}_{scale} + \beta \mathcal{L}_{mask} + \gamma \mathcal{L}_{GAN}, \quad (1)$$

where α , φ , β and γ are the balance factors between loss terms. \mathcal{L}_{scale} refers to the proposed scale consistency loss, and \mathcal{L}_{mask} is a regularization term to constrain the training of

MaskNet, which is inspired by Zhou *et al.* [3]. \mathcal{L}_{GAN} denotes the adversarial loss. \mathcal{L}_{basic} stands for the basic loss. The basic loss is used to assist the training process of generator and consists of three parts, the traditional reconstruction loss \mathcal{L}_{rec} , the smoothness loss \mathcal{L}_{smooth} :

$$\mathcal{L}_{basic} = \alpha_1 \mathcal{L}_{rec} + \alpha_2 \mathcal{L}_{smooth}, \quad (2)$$

where α_1 and α_2 are the balance factors.

Reconstruction Loss: With the output of DepthNet and PoseNet, the target images can be reconstructed from the source images I_s through the view reconstruction algorithm, which is widely used in previous unsupervised monocular depth estimation framework [3], [9], [26]. The principle of this algorithm is based on the projection function:

$$p_s \sim K \hat{T}_{t \rightarrow s} \hat{D}_t(p_t) K^{-1} p_t, \quad (3)$$

where K stands for the camera intrinsics matrix. \hat{D}_t denotes the depth estimation of target image I_t , and $\hat{T}_{t \rightarrow s}$ represents the predicted 6-DOF transformation between the target image I_t and source image I_s . The pixels of two images p_t, p_s establish the correspondence by projection function. Then, we synthesize \hat{I}_s by warping I_s and differentiable bilinear interpolation. Finally, the reconstruction loss is formulated as:

$$\mathcal{L}_{rec} = \alpha_3 \frac{1 - SSIM(I_t, \hat{I}_s)}{2} - (1 - \alpha_3) \|I_t - \hat{I}_s\|_1, \quad (4)$$

where α_3 refers to a balance factor, and SSIM [27] is an index that shows the structure similarity between I_t and \hat{I}_s .

Smoothness Loss: In order to filter out erroneous predictions and promote the representation of geometric structure, a smoothness loss is designed to constrain the smoothness of the predicted depth map. Following our previous works [42], we adopt the second-order differential for improving

the smoothness, which is different from recent unsupervised monocular frameworks [9], [25], [26]:

$$\mathcal{L}_{smooth} = \sum_{p_t} |\nabla(\nabla D(p_t))| (e^{-|\nabla p_t|})^T, \quad (5)$$

where ∇ denotes the vector differential operator, and T is the transpose operation.

Traditional mask for reconstruction loss: In order to eliminate the influence of visual field changes and dynamic objects on reconstruction loss, we use a MaskNet to predict these unreconstructed regions. During training, a MaskNet is designed to estimate different regions between the target image I_t and the synthesized image \hat{I}_s , formatted as $\min[M \times (I_t - \hat{I}_s)]$, and a regularization term \mathcal{L}_{mask} is used to constrain the MaskNet during training, which is similar to [3]. Our intention is to use the MaskNet to predict the regions that could not be reconstructed. Considering the effect of incomplete reconstruction on reconstruction loss, the mask M predicted by MaskNet is introduced into \mathcal{L}_{rec}^m :

$$\mathcal{L}_{rec}^m = \sum_{p_t} M \mathcal{L}_{rec}. \quad (6)$$

Our final basic model with mask is formulated as follow:

$$\mathcal{L}_{basic}^m = \alpha_1 \mathcal{L}_{rec}^m + \alpha_2 \mathcal{L}_{smooth}. \quad (7)$$

Scale Consistency Loss: In the unsupervised monocular frameworks, the depth and pose networks are trained by the unlabelled short frame snippets that consisting of 3 or 5 frames. During training, because of the projection constraints and reconstruction loss, the poses ($T_{t,s1}$, $T_{t,s2}$) between target image I_t and source images I_{s1} , I_{s2} regressed by pose network have the same scale factor in a snippet. However, different snippets have different scale factors (compared with the ground truth) because there is no corresponding scale constraint loss applied. Therefore, previous pose and depth networks [3], [9] cannot provide scale-consistent results between different snippets. Bian *et al.* [26] consider the scale-consistency of pose network for generating full trajectories over long monocular videos. Similarly, this paper proposes a novel adaptive loss for better constraint on geometric and scale consistency between snippets, which is formulated as follows:

$$\mathcal{L}_{scale} = \alpha_4 \frac{1 - SSIM(D_s^t, \hat{D}_s^s)}{2} - (1 - \alpha_4) \|D_s^t - \hat{D}_s^s\|_1, \quad (8)$$

$$D_s^t(p_s) \sim K \hat{T}_{t \rightarrow s} \hat{D}_t(p_t) K^{-1} p_t, \quad (9)$$

where α_4 refers to a balance factor. $D_s^t(p_s)$ is computed by the projection algorithm shown in Eq. (9), and it has the same scale information as \hat{D}_t . \hat{D}_t stands for the predicted depth map of target image. \hat{D}_s is the predicted depth map of source image (the target image of next frame snippet). \hat{D}_s^s is reconstructed from \hat{D}_s by warping algorithm, which is similar to the view reconstruction process in [3], and it contains the same scale information as \hat{D}_s . Then, SSIM loss [27] is adopted for the consistency of D_s^t and \hat{D}_s^s so that the scale between snippets is aligned.

C. Boolean mask processing for masked GAN

Original GAN consists of two components, a generator (G) and a discriminator (D) [41]. The discriminator is designed to distinguish the real data x and synthesized data $G(z)$ by learning the distribution of them. Meanwhile, the major task of generator is to generate a set of data $G(z)$ with the same distribution as the real data to fool the discriminator. Therefore, a max-min game is played between the generator and discriminator, and the loss function of original GAN [41] is formulated as:

$$\begin{aligned} \mathcal{L} &= \min_G \max_D V(D, G) \\ &= \mathbb{E}_{x \sim p_{data}(x)} [\log D(x)] \mathbb{E}_{z \sim p_z(z)} [\log(1 - D(G(z)))], \end{aligned} \quad (10)$$

where $p_{data}(x)$ and $p_z(z)$ stand for the data distribution of x and z , respectively. Finally, a mapping relationship between two data distributions is established through adversarial learning.

The unsupervised monocular depth estimation cannot feed the discriminator with real depth map because there is no ground truth. To deal with this, the framework combined with GANs is proposed in previous works to predict depth and ego-motion [17], [20]. The RGB images synthesized \hat{I}_s by the view reconstruction are sent to discriminator together with the target images I_t :

$$\begin{aligned} \mathcal{L}_{GAN} &= \min_G \max_D V(D, G) \\ &= \mathbb{E}_{I_t \sim p(I_t)} [\log D(I_t)] + \mathbb{E}_{\hat{I}_s \sim p(\hat{I}_s)} [\log(1 - D(\hat{I}_s))], \end{aligned} \quad (11)$$

where $D(\cdot)$ and $G(\cdot)$ stand for the discriminator and generator of this paper.

Since the data distribution of unreconstructed regions is unique to synthetic images, which will affect the adversarial learning, we propose a boolean mask to reduce the impact of unreconstructed regions on adversarial learning, and the same unreconstructed regions as synthetic images are produced on target images.

Boolean mask processing: Firstly, we transfer the floating point mask M predicted by MaskNet to a boolean type M_b by comparing with a threshold θ :

$$M_b(p) = \begin{cases} 0 & \text{if } |M(p)| \leq \theta, \\ 1 & \text{if } |M(p)| > \theta, \end{cases} \quad (12)$$

where p stands for the pixel index on the mask. Then, to eliminate the distinctive feature (unreconstructed regions in synthesized images) between synthesized and target images, we use the boolean mask M_b to reweight target image I_t and make similar unreconstructed regions as the synthesized image \hat{I}_s on the target image I_t :

$$I_t^{M_b} = M_b I_t. \quad (13)$$

Besides, to prevent this boolean mask processing step from introducing the new and particular noises into target images to influence the training of discriminator, we do the same boolean mask processing operation to the synthesized image \hat{I}_s :

$$\hat{I}_s^{M_b} = M_b \hat{I}_s. \quad (14)$$

Masked GAN: After preprocessing by the boolean mask, the masked target (real) and synthesized (fake) images, $I_t^{M_b}$ and

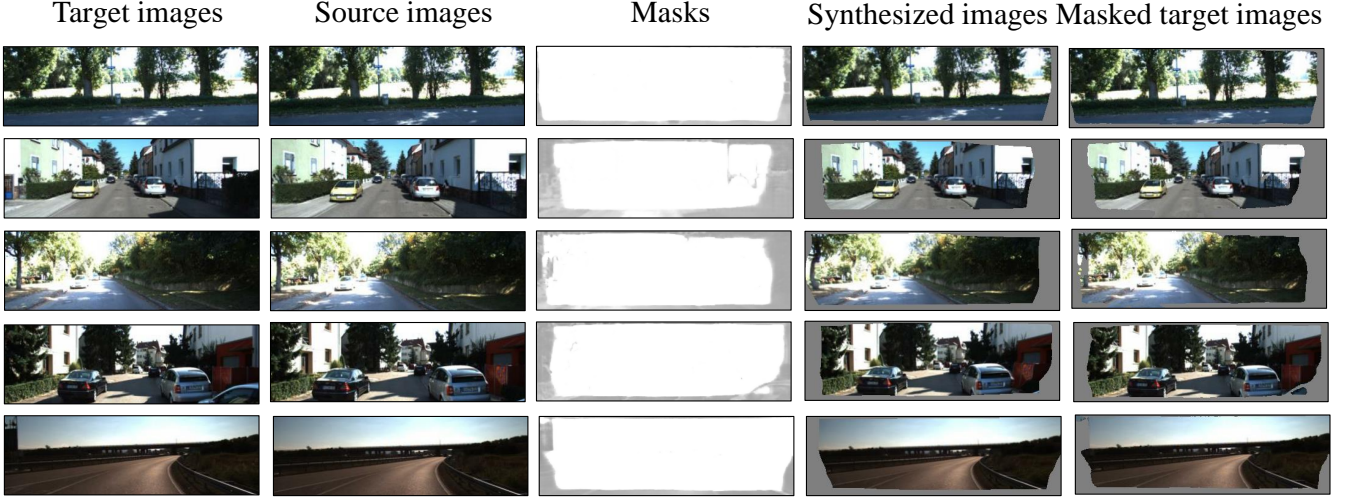


Fig. 4. Qualitative results of MaskNet and boolean mask processing. The “masks” are generated by MaskNet to predict unreconstructed regions on synthesized images, and they are converted to the boolean one to preprocess the target image. The “synthesized images” are reconstructed from source images by view reconstruction algorithm. The “masked target images” are preprocessed by boolean mask and have the similar empty regions to synthesized images.

$\hat{I}_s^{M_b}$, are sent to the discriminator, and our final adversarial loss is formulated as follows:

$$\begin{aligned} \mathcal{L}_{GAN}^{M_b} &= \min_G \max_D V(D, G) \\ &= \mathbb{E}_{I_t^{M_b} \sim p(I_t^{M_b})} [\log D(I_t^{M_b})] + \mathbb{E}_{\hat{I}_s^{M_b} \sim p(\hat{I}_s^{M_b})} [\log(1 - D(G(I_t, I_s)))] \\ &= \mathbb{E}_{I_t^{M_b} \sim p(I_t^{M_b})} [\log D(I_t^{M_b})] + \mathbb{E}_{\hat{I}_s^{M_b} \sim p(\hat{I}_s^{M_b})} [\log(1 - D(\hat{I}_s^{M_b}))], \end{aligned} \quad (15)$$

where $I_t^{M_b}$ and $\hat{I}_s^{M_b}$ are calculated by boolean mask processing, Eq.13 and Eq. 14.

Floating point mask processing: To verify the effectiveness of boolean mask processing, instead of transferring the mask to the boolean one, the floating point mask $M_f = M$ predicted by MaskNet is directly used to preprocess the synthesized and target image (\hat{I}_s, I_t):

$$\hat{I}_s^{M_f} = M_f \hat{I}_s, \quad I_t^{M_f} = M_f I_t. \quad (16)$$

Therefore, the adversarial loss combined with floating point mask processing is formulated as:

$$\begin{aligned} \mathcal{L}_{GAN}^{M_f} &= \min_G \max_D V(D, G) \\ &= \mathbb{E}_{I_t^{M_f} \sim p(I_t^{M_f})} [\log D(I_t^{M_f})] + \mathbb{E}_{\hat{I}_s^{M_f} \sim p(\hat{I}_s^{M_f})} [\log(1 - D(\hat{I}_s^{M_f}))], \end{aligned} \quad (17)$$

where $I_t^{M_f}$ and $\hat{I}_s^{M_f}$ are calculated by floating point mask processing, Eq.16.

IV. EXPERIMENTS

A. Implementation Details

Network architecture: Our unsupervised method mainly consists of two modules, generator and discriminator, which can be divided into three subnetworks, the MaskNet coupled with the PoseNet, the DepthNet, and the discriminator network. Our MaskNet and DepthNet follow the traditional encoder-decoder framework. Previous works [9], [10], [26] have shown the good performance of DispResNet [9] so that

we choose it as our DepthNet. The input of DepthNet is a single RGB image, and the depth map is predicted in an end-to-end manner. For the mask network, the MaskNet is coupled with a PoseNet, which is a widely adopted framework in previous works [3], [25]. The main difference is that we add the skip-connection like [43] between encoder and decoder to preserve important information [44] and improve the performance of mask prediction. Besides, the MaskNet predicts a mask to handle occlusions, dynamic objects and visual field changes between target and source images. The architecture of discriminator network is designed with reference to the encoder of DispNet [45]. The target images and synthesized images are both preprocessed by boolean mask processing step before being sent to the discriminator. During training, the discriminator outputs the probability that the input image is real or fake, and the adversarial learning between the generator and discriminator improves the training of depth and pose networks.

Training detail: The training of our networks is based on Tensorflow framework [46] and lasts about 28 hours on a NVIDIA RTX 2080TI GPU. We use the KITTI raw dataset [28] to train our DepthNet, and sequences 00-08 of the KITTI odometry dataset are applied to train our PoseNet. For fairness, the usage of training and testing sets is the same as previous works [3], [9], [10], [20], [26]. During training, the image resolution is resized to 416×128 , the weights of generator and discriminator are optimized by ADAM optimizers [47] with $\beta_1 = 0.9$, $\beta_2 = 0.999$, learning rate of 0.0002 and batch size of 4. During training, we adopt $\alpha_1 = 1.0$, $\alpha_2 = 0.5$, $\alpha_3 = 0.85$, $\alpha_4 = 0.2$, $\varphi = 0.5$, $\beta = 0.4$, $\gamma = 0.001$, $\theta = 0.9$. We only fine-tune the β and γ , and the other parameters are set based on experiments or related works. We set the length of frame snippets to be 5 for training DepthNet and 3 for PoseNet to get better results. We directly use the pose estimation between adjacent frames predicted by PoseNet to generate a global trajectory of the testing sequence.

Evaluation metrics: For depth evaluation, the commonly

TABLE I

ABLATION STUDY RESULTS ON THE KITTI RAW DATASET [28]. BASED ON THE BASIC LOSS FUNCTION (\mathcal{L}_{basic} , EQ. (2)), SCALE CONSISTENCY LOSS (\mathcal{L}_{scale} , EQ. (8)), ADVERSARIAL LEARNING (\mathcal{L}_{GAN} , EQ. (11)), MASKS FOR RECONSTRUCTION LOSS (\mathcal{L}_{basic}^m , EQ. (7), \mathcal{L}_{mask}), FLOATING POINT MASK PROCESSING FOR ADVERSARIAL LEARNING (\mathcal{L}_{GAN}^{Mf} , EQ. (17)), AND BOOLEAN MASK PROCESSING FOR ADVERSARIAL LEARNING (\mathcal{L}_{GAN}^{Mb} , EQ. (15)) ARE INTRODUCED SEQUENTIALLY INTO TRAINING.

Method	Resolution	Lower is better				Higher is better		
		Abs Rel	Sq Rel	RMSE	RMSE log	$\delta < 1.25^1$	$\delta < 1.25^2$	$\delta < 1.25^3$
\mathcal{L}_{basic}	416×128	0.154	1.287	5.918	0.236	0.796	0.925	0.970
$\mathcal{L}_{basic} + \mathcal{L}_{scale}$	416×128	0.153	1.173	5.573	0.228	0.796	0.931	0.974
$\mathcal{L}_{basic} + \mathcal{L}_{scale} + \mathcal{L}_{GAN}$	416×128	0.152	1.142	5.630	0.230	0.791	0.928	0.973
$\mathcal{L}_{basic}^m + \mathcal{L}_{scale} + \mathcal{L}_{GAN} + \mathcal{L}_{mask}$	416×128	0.149	1.093	5.589	0.226	0.796	0.930	0.974
$\mathcal{L}_{basic}^m + \mathcal{L}_{scale} + \mathcal{L}_{GAN}^{Mf} + \mathcal{L}_{mask}$	416×128	0.150	1.138	5.557	0.226	0.797	0.931	0.974
$\mathcal{L}_{basic}^m + \mathcal{L}_{scale} + \mathcal{L}_{GAN}^{Mb} + \mathcal{L}_{mask}$	416×128	0.148	1.091	5.536	0.209	0.802	0.934	0.976

TABLE II

COMPARISON WITH THE METHODS USING GANs FOR UNSUPERVISED MONOCULAR DEPTH AND VO ESTIMATION. “SC” STANDS FOR WHETHER THE SCALE-CONSISTENT IS CONSIDERED IN THEIR WORK. * - DENOTES THAT THEIR DEPTH MAP IS NOT GENERATED FROM A SINGLE IMAGE IN AN END-TO-END MANNER.

Method	Resolution	SC	Lower is better				Higher is better		
			Abs Rel	Sq Rel	RMSE	RMSE log	$\delta < 1.25^1$	$\delta < 1.25^2$	$\delta < 1.25^3$
Kumar <i>et al.</i> [17]	384×128	×	0.211	1.980	6.154	0.264	0.732	0.898	0.959
GANVO * [20]	416×128	×	0.150	1.141	5.448	0.216	0.808	0.939	0.975
Li <i>et al.</i> * [25]	416×128	✓	0.150	1.127	5.564	0.229	0.823	0.936	0.974
OURS	416×128	✓	0.148	1.091	5.536	0.209	0.802	0.934	0.976

used evaluation metrics proposed by Eigen *et al.* [1] is used in this paper to compare with others fairly, which include five evaluation indicators: **RMSE**, **RMSE log**, **Abs Rel**, **Sq Rel**, **Accuracy**:

- **RMSE** = $\sqrt{\frac{1}{|N|} \sum_{i \in N} \|d_i - d_i^*\|^2}$,
- **RMSE log** = $\sqrt{\frac{1}{|N|} \sum_{i \in N} \|\log(d_i) - \log(d_i^*)\|^2}$,
- **Abs Rel** = $\frac{1}{|N|} \sum_{i \in N} \frac{|d_i - d_i^*|}{d_i^*}$,
- **Sq Rel** = $\frac{1}{|N|} \sum_{i \in N} \frac{\|d_i - d_i^*\|^2}{d_i^*}$,
- **Accuracy**: % of d_i s.t. $\max(\frac{d_i}{d_i^*}, \frac{d_i^*}{d_i}) = \delta < thr$,

where d_i and d_i^* denote the predicted depth of pixel i and corresponding ground truth, and N denotes the total number of the corresponding pixels with ground truth depth value. thr denotes a threshold, and it is always set to 1.25^1 , 1.25^2 , and 1.25^3 during evaluation.

For trajectory evaluation, the generated full trajectory is evaluated by the standard evaluation metrics provided in the dataset [28], including a translation error metric $t_{err}(\%)$ and a rotation error metric $r_{err}(^\circ/100m)$. Compared with the 5-frame pose evaluation that is proposed in [3], the evaluation metrics in this paper are more widely used in traditional VO methods and more meaningful.

B. Monocular Depth Estimation

Ablation study: In this section, we first conduct a series of ablation experiments to validate the efficacy of our proposed framework, as shown in Table I. The “ \mathcal{L}_{basic} ” denotes that our framework is trained by the basic loss \mathcal{L}_{basic} (Eq. (2)), which consists of the reconstruction loss (\mathcal{L}_{rec} , Eq. (4)), and smoothness loss (\mathcal{L}_{smooth} , Eq. (5)). Then, scale consistency loss (\mathcal{L}_{scale} , Eq. (8)), adversarial learning (\mathcal{L}_{GAN} , Eq. (11)), masks for reconstruction loss (\mathcal{L}_{basic}^m , Eq. (7), \mathcal{L}_{mask}), and

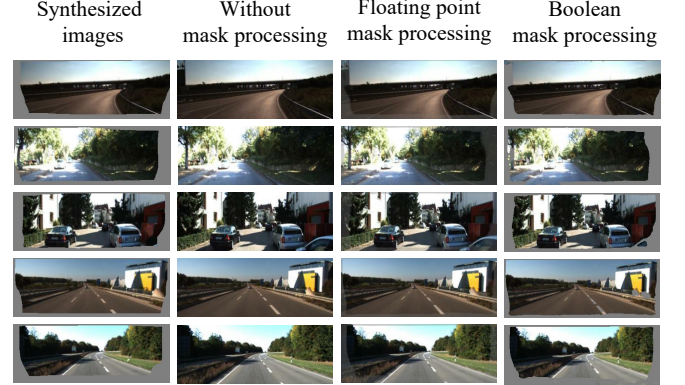


Fig. 5. Visual results of different kinds of mask processing. Raw mask processing can only dilute the view while boolean mask processing is able to construct empty regions that are almost identical to synthesized images.

boolean mask processing (\mathcal{L}_{GAN}^{Mb} , Eq. (15)) are introduced sequentially into training. Although both mask and boolean mask processing (BMP) in Table I are based on the output of MaskNet, the mask is to reduce the effect of unreconstructed regions on reconstruction loss, while BMP is applied to eliminate the impact of unreconstructed regions on adversarial loss.

From the results shown in Table I, comparing lines 1 and 2 in the table, the proposed scale consistency loss \mathcal{L}_{scale} is conducive to the improvement of depth estimation. Comparing lines 2 and 3, the introduction of adversarial learning (GAN) does not improve the accuracy of depth network, i.e., the introduced adversarial learning does not play a role in the training of DepthNet. On the other hand, we achieve a surprising good result when the BMP is used to reduce the impact of unreconstructed regions on adversarial learning. Therefore, we believe

TABLE III

MONOCULAR DEPTH RESULTS ON KITTI [28] BY THE SPLIT OF EIGEN *et al.* [1]. FOR TRAINING, MONO. /STEREO DENOTES THAT NETWORKS TRAINED BY MONOCULAR SEQUENCES / STEREO IMAGE PAIRS. “-RESNET” STANDS FOR THE METHODS WITH DISPRESNET [9]. WE SHOW THE BEST RESULTS IN BOLD.

Method	Supervision	Resolution	Cap	Lower is better				Higher is better		
				Abs Rel	Sq Rel	RMSE	RMSE log	$\delta < 1.25^1$	$\delta < 1.25^2$	$\delta < 1.25^3$
SfMLearner [3]	Mono.	416×128	80m	0.208	1.768	6.865	0.283	0.678	0.885	0.957
Yang <i>et al.</i> [48]	Mono.	416×128	80m	0.182	1.481	6.501	0.267	0.725	0.906	0.963
Vid2depth [49]	Mono.	416×128	80m	0.163	1.240	6.220	0.250	0.762	0.916	0.968
GeoNet-ResNet. [9]	Mono.	416×128	80m	0.155	1.296	5.857	0.233	0.793	0.931	0.973
Wang <i>et al.</i> [35]	Mono.	416×128	80m	0.154	1.163	5.700	0.229	0.792	0.932	0.974
SC-SfM-ResNet [26]	Mono.	416×128	80m	0.149	1.137	5.771	0.230	0.799	0.932	0.973
OURS	Mono	416×128	80m	0.148	1.091	5.536	0.209	0.802	0.934	0.976
DF-Net [37]	Mono.	576×160	80m	0.150	1.124	5.507	0.223	0.806	0.933	0.973
CC [10]	Mono.	832×256	80m	0.140	1.070	5.326	0.217	0.826	0.941	0.975
SC-SfM [26]	Mono.	832×256	80m	0.137	1.089	5.439	0.217	0.830	0.942	0.975
Vid2depth [49]	Mono.	416×128	50m	0.155	0.927	4.549	0.231	0.781	0.931	0.975
GeoNet-ResNet. [9]	Mono.	416×128	50m	0.147	0.889	4.290	0.214	0.808	0.942	0.979
Wang <i>et al.</i> [35]	Mono.	416×128	50m	0.154	1.163	5.700	0.229	0.792	0.932	0.974
OURS	Mono.	416×128	50m	0.141	0.848	4.204	0.209	0.818	0.944	0.980
Godard <i>et al.</i> [33]	Stereo	512×256	50m	0.140	0.976	4.471	0.232	0.818	0.937	0.973
Zhan <i>et al.</i> [34]	Stereo	608×160	50m	0.128	0.815	4.204	0.216	0.818	0.941	0.975

that the unreconstructed regions influence the performance of adversarial learning. Then, the mask predicted by MaskNet is introduced into the framework, shown as “ $\mathcal{L}_{basic}^m + \mathcal{L}_{scale} + \mathcal{L}_{GAN} + \mathcal{L}_{mask}$ ”. From the evaluation metrics, the depth estimation accuracy of “ $\mathcal{L}_{basic}^m + \mathcal{L}_{scale} + \mathcal{L}_{GAN} + \mathcal{L}_{mask}$ ” outperforms that of “ $\mathcal{L}_{basic} + \mathcal{L}_{scale} + \mathcal{L}_{GAN}$ ”, which means that the adopted mask improves the training process of the network. With the qualitative results of mask in Fig. 4, the unreconstructed regions of synthesized images are accurately predicted in the masks. Therefore, the reason for accuracy improvement in depth estimation is that the mask is able to significantly mitigate the influence of unreconstructed regions on reconstruction loss. Afterwards, we adopt the BMP in this paper to mask the target (real) and synthesized (fake) images before sending to discriminator, shown as “ $\mathcal{L}_{basic}^m + \mathcal{L}_{scale} + \mathcal{L}_{GAN}^{M_b} + \mathcal{L}_{mask}$ ”, and the best result among four cases is achieved. Besides, the qualitative results of BMP shown in Fig. 4 also demonstrate that our proposed BMP can construct the similar unreconstructed regions in target images, which helps to reduce the impact of unreconstructed regions on adversarial learning and plays a key role in adversarial learning. In summary, this ablation study indicates the effectiveness of our proposed modules.

Comparison of different mask processing: To further verify the ability of the boolean mask, we compare the GAN processed by BMP ($\mathcal{L}_{GAN}^{M_b}$) with the cases of GAN processed by floating point mask (FMP) ($\mathcal{L}_{GAN}^{M_f}$) and the original GAN without mask processing (\mathcal{L}_{GAN}), and the results are shown in lines 4, 5 and 6 of Table I. Although FMP cannot create the similar unreconstructed regions on target images as synthesized images, it can be seen from Table I that FMP plays a positive role in improving the performance of adversarial learning when compared with the original GAN. As the examples of different mask processing results shown in Fig. 5, the effect of FMP is not as obvious as BMP. Besides, experimental results in Table I show that either FMP or BMP are effective in accuracy improvement of depth estimation, and BMP works the best.

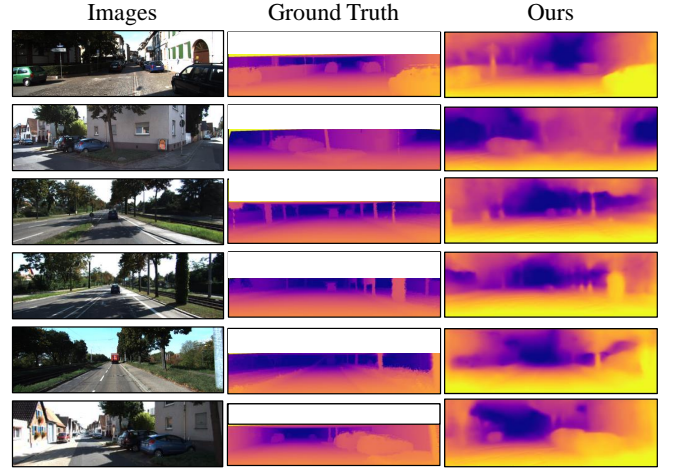


Fig. 6. Qualitative results of our depth networks, which is trained in an unsupervised manner. The geometric structures in the scenes, such as boles and cars, can be effectively presented by our depth model from single images.

Comparison with the methods using GANs: We compare with the unsupervised monocular methods proposed in [17], [20], [25], which introduce adversarial learning into the training framework. Note that the GANVO [20] generates its depth prediction from a vector, which means that their depth network cannot be used independently and predict depth in an end-to-end manner. Meanwhile, the depth network in [25] takes a single image as well as the temporal information for depth estimation, therefore this network takes more information than ours in depth estimation. Besides, because of the LSTM module used in their framework in [25], the accuracy of depth network depends on images sequences, and depth network cannot predict the depth map from only a single image, which limits its practical applications. Although our DepthNet is jointly trained with other networks in the unsupervised manner, it can be used independently during testing and has the ability to accurately generate depth maps from single images, which enables it to perform depth estimation on some

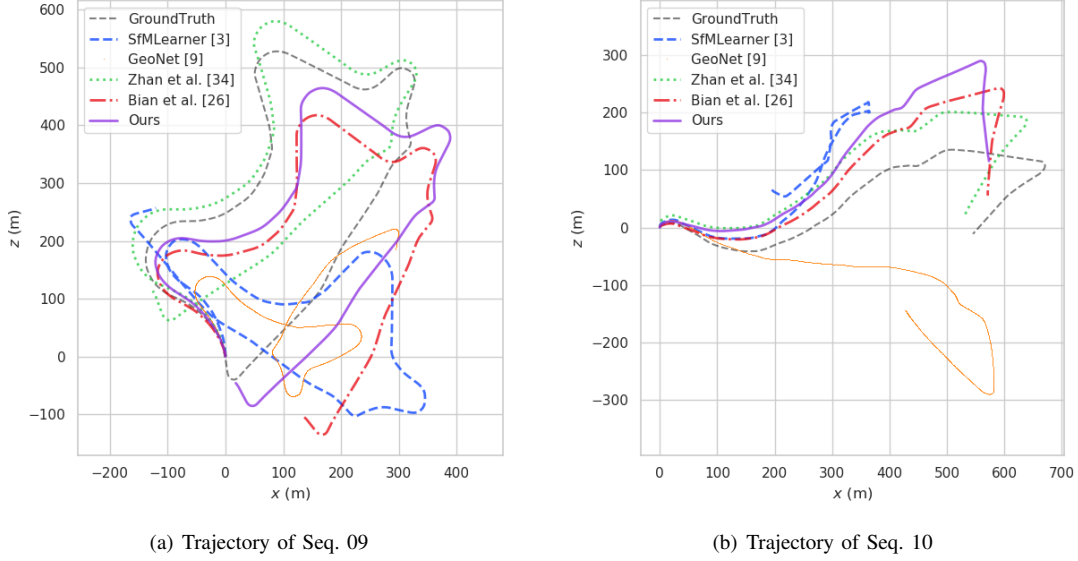


Fig. 7. Qualitative results on the testing sequences of KITTI odometry dataset.

independent images such as network images. The quantitative results are shown in Table II, and our method obtain the competitive results.

Comparison with previous works: Considering that a lot of previous works [9], [10], [26] have shown that Disp-ResNet [9] has a better performance than DispNet [3], [45], we take the Disp-ResNet as our DepthNet. The qualitative and quantitative results of our DepthNet are evaluated by the public metrics and shown in Fig. 6 and Table III. Compared the ground truth with our predicted depth maps in Fig. 6, our deep network predicts the depth information of geometric structures in the scenes, such as trees, streets, cars, and buildings, etc. Note that higher resolutions include detailed geometric details, so we divided the results of different methods according to the resolution of their input images for fairness. It has been proved that the high-resolution input is conducive to the improvement of accuracy [26]. Therefore, we choose images with a resolution of 416×128 as the input to the DepthNet, therefore our depth network can fit more cameras. As shown in Table III, we obtain a better performance on end-to-end monocular depth prediction under the condition that the resolution is 416×128 . In addition, our DepthNet also gets competitive results when compared to the stereo methods [33], [34].

C. Trajectory Prediction

For PoseNet, we follow Zhan *et al.* [34] and Bian *et al.* [26] and evaluate the sequence 09-10 of the KITTI Odometry sequence. The standard evaluation tools provided by the dataset are used to evaluate the full predicted trajectories, which are different from previous monocular DL-based pose evaluation methods [3], [9], [10], [21]. Table IV shows the average rotation and translation errors of predicted trajectories on the KITTI odometry sequence 09 and 10. As shown in Table IV, comparing the results of “OURS-ResNet(Without \mathcal{L}_{scale})” and “OURS-ResNet”, the proposed scale consistency loss \mathcal{L}_{scale}

TABLE IV
VISUAL ODOMETRY RESULTS ON KITTI ODOMETRY DATASET [28]

Method	Supervision	Seq. 09		Seq. 10	
		$t_{err}(\%)$	$r_{err}(^\circ/100m)$	$t_{err}(\%)$	$r_{err}(^\circ/100m)$
ORB-SLAM [14]	-	15.30	0.26	3.68	0.48
SfMLearner [3]	Mono.	17.84	6.78	37.91	17.78
GeoNet [9]	Mono.	41.47	13.14	32.74	13.12
Zhan <i>et al.</i> [34]	Stereo.	11.93	3.91	12.45	3.46
Bian <i>et al.</i> [26]	Mono.	11.2	3.35	10.1	4.96
Wang <i>et al.</i> [51]	Mono.	9.88	3.40	12.24	5.20
OURS-ResNet(Without \mathcal{L}_{scale})	Mono.	12.75	4.25	14.45	4.33
OURS-ResNet	Mono.	10.54	3.52	11.1	3.79
OURS-VGG	Mono.	8.99	3.24	11.09	5.34

is effective to constrain the scale consistency. Although the method in [25] also considers the scale-inconsistency of pose estimation, the generated trajectories are neither evaluated in the article nor published online, so we cannot make a quantitative comparison with their trajectories. The visual results are shown in Fig. 7, which are drawn by evo tools [50] with automatic scale alignment for full trajectory. The method [34] trained with stereo image pairs does not have the problem of scale inconsistency because it learns the scale information when training from stereo data. Monocular methods [3], [9], [51] train their network with monocular sequence and suffer from per-pose scale ambiguity and inconsistency. Meanwhile, the scale information between different snippets predicted by PoseNet is inconsistent so that they cannot provide an accurate trajectory. Bian *et al.* tackle this problem by the geometric alignment, and our method is shown to be competitive with them.

Besides, as shown in Table IV, because of the strong back-end optimization, ORB-SLAM [14] shows more powerful performance in position and orientation prediction than deep learning-based VO methods. Although there is still a big gap compared with the traditional VO method [14], our pose network has the ability to predict the full trajectory over long monocular video in an end-to-end manner. With the continuous development of deep networks and the application of novel

geometric constraints, we believe that end-to-end trajectory planning based on deep learning will eventually outperform traditional methods.

V. CONCLUSION

In this paper, we present an unsupervised monocular depth and VO estimation framework with scale consistency through adversarial learning methods. The proposed method considers the impact of incomplete reconstruction caused by dynamic objects, occlusions and visual field changes on reconstruction loss and adversarial loss, which in turn affects the training of discriminator and generator networks. This paper tackles these problems by introducing a MaskNet. The mask predicted by MaskNet is used to reduce the impact of incomplete reconstruction on reconstruction loss. Besides, we design a BMP to preprocess real images to produce the same data distribution as unreconstructed areas on synthesized images, thus restoring balance to the generator and discriminator. Furthermore, we tackle the scale-inconsistency in pose and depth estimation by introducing an adaptive constraint. With the proposed adversarial learning framework, our depth model shows competitive results with the state-of-the-art methods, and our pose model has the ability to provide a global trajectory over long monocular sequence, which is meaningful for practical applications. In the future, we will improve the geometric constraints for more accurate trajectory prediction.

REFERENCES

- [1] D. Eigen, C. Puhrsch, and R. Fergus, "Depth map prediction from a single image using a multi-scale deep network," in *Advances in Neural Information Processing Systems*, 2014, pp. 2366–2374.
- [2] J. Liu, Y. Wang, Y. Li, J. Fu, J. Li, and H. Lu, "Collaborative deconvolutional neural networks for joint depth estimation and semantic segmentation," *IEEE transactions on neural networks and learning systems*, vol. 29, no. 11, pp. 5655–5666, 2018.
- [3] T. Zhou, M. Brown, N. Snavely, and D. G. Lowe, "Unsupervised learning of depth and ego-motion from video," in *Proceedings of the IEEE Conference on Computer Vision and Pattern Recognition*, 2017, pp. 1851–1858.
- [4] Q. Sun, Y. Tang, and C. Zhao, "Cycle-sfm: Joint self-supervised learning of depth and camera motion from monocular image sequences," *Chaos: An Interdisciplinary Journal of Nonlinear Science*, vol. 29, no. 12, p. 123102, 2019.
- [5] Y. Tang, C. Zhao, J. Wang, C. Zhang, Q. Sun, W. Zheng, W. Du, F. Qian, and J. Kurths, "An overview of perception and decision-making in autonomous systems in the era of learning," *arXiv preprint arXiv:2001.02319*, 2020.
- [6] C. Zhao, Q. Sun, C. Zhang, Y. Tang, and F. Qian, "Monocular depth estimation based on deep learning: An overview," *arXiv preprint arXiv:2003.06620*, 2020.
- [7] J. Jiao, Y. Cao, Y. Song, and R. Lau, "Look deeper into depth: Monocular depth estimation with semantic booster and attention-driven loss," in *Proceedings of the European Conference on Computer Vision (ECCV)*, 2018, pp. 53–69.
- [8] P.-Y. Chen, A. H. Liu, Y.-C. Liu, and Y.-C. F. Wang, "Towards scene understanding: Unsupervised monocular depth estimation with semantic-aware representation," in *Proceedings of the IEEE Conference on Computer Vision and Pattern Recognition*, 2019, pp. 2624–2632.
- [9] Z. Yin and J. Shi, "GeoNet: Unsupervised learning of dense depth, optical flow and camera pose," in *Proceedings of the IEEE Conference on Computer Vision and Pattern Recognition*, 2018, pp. 1983–1992.
- [10] A. Ranjan, V. Jampani, L. Balles, K. Kim, D. Sun, J. Wulff, and M. J. Black, "Competitive Collaboration: Joint Unsupervised Learning of Depth, Camera Motion, Optical Flow and Motion Segmentation," in *Proceedings of the IEEE Conference on Computer Vision and Pattern Recognition*, 2019, pp. 12240–12249.
- [11] N. Snavely, S. M. Seitz, and R. Szeliski, "Modeling the world from internet photo collections," *International Journal of Computer Vision*, vol. 80, no. 2, pp. 189–210, 2008.
- [12] C. Forster, Z. Zhang, M. Gassner, M. Werlberger, and D. Scaramuzza, "SVO: Semidirect visual odometry for monocular and multicamera systems," *IEEE Transactions on Robotics*, vol. 33, no. 2, pp. 249–265, 2016.
- [13] J. Engel, V. Koltun, and D. Cremers, "Direct sparse odometry," *IEEE Transactions on Pattern Analysis and Machine Intelligence*, vol. 40, no. 3, pp. 611–625, 2017.
- [14] R. Mur-Artal and J. D. Tardós, "Orb-slam2: An open-source slam system for monocular, stereo, and rgb-d cameras," *IEEE Transactions on Robotics*, vol. 33, no. 5, pp. 1255–1262, 2017.
- [15] B. Triggs, P. F. McLauchlan, R. I. Hartley, and A. W. Fitzgibbon, "Bundle adjustment modern synthesis," in *International Workshop on Vision Algorithms*. Springer, 1999, pp. 298–372.
- [16] J. Zhang and C. Li, "Adversarial examples: Opportunities and challenges," *IEEE transactions on neural networks and learning systems*, 2019.
- [17] A. CS Kumar, S. M. Bhandarkar, and M. Prasad, "Monocular depth prediction using generative adversarial networks," in *Proceedings of the IEEE Conference on Computer Vision and Pattern Recognition Workshops*, 2018, pp. 300–308.
- [18] K. Gwn Lore, K. Reddy, M. Giering, and E. A. Bernal, "Generative adversarial networks for depth map estimation from rgb video," in *Proceedings of the IEEE Conference on Computer Vision and Pattern Recognition Workshops*, 2018, pp. 1177–1185.
- [19] F. Aleotti, F. Tosi, M. Poggi, and S. Mattoccia, "Generative Adversarial Networks for Unsupervised Monocular Depth Prediction," in *European Conference on Computer Vision*. Springer, 2018, pp. 337–354.
- [20] Y. Almalioglu, M. R. U. Saputra, P. P. de Gusmao, A. Markham, and N. Trigoni, "GANVO: Unsupervised deep monocular visual odometry and depth estimation with generative adversarial networks," in *2019 International Conference on Robotics and Automation (ICRA)*. IEEE, 2019, pp. 5474–5480.
- [21] T. Feng and D. Gu, "Sganvo: Unsupervised deep visual odometry and depth estimation with stacked generative adversarial networks," *arXiv preprint arXiv:1906.08889*, 2019.
- [22] S. Zhao, H. Fu, M. Gong, and D. Tao, "Geometry-Aware Symmetric Domain Adaptation for Monocular Depth Estimation," in *Proceedings of the IEEE Conference on Computer Vision and Pattern Recognition*, 2019, pp. 9788–9798.
- [23] H. Jung, Y. Kim, D. Min, C. Oh, and K. Sohn, "Depth prediction from a single image with conditional adversarial networks," in *2017 IEEE International Conference on Image Processing (ICIP)*. IEEE, 2017, pp. 1717–1721.
- [24] A. Pilzer, D. Xu, M. Puscas, E. Ricci, and N. Sebe, "Unsupervised adversarial depth estimation using cycled generative networks," in *2018 International Conference on 3D Vision (3DV)*. IEEE, 2018, pp. 587–595.
- [25] S. Li, F. Xue, X. Wang, Z. Yan, and H. Zha, "Sequential adversarial learning for self-supervised deep visual odometry," in *Proceedings of the IEEE International Conference on Computer Vision*, 2019, pp. 2851–2860.
- [26] J.-W. Bian, Z. Li, N. Wang, H. Zhan, C. Shen, M.-M. Cheng, and I. Reid, "Unsupervised scale-consistent depth and ego-motion learning from monocular video," in *Thirty-third Conference on Neural Information Processing Systems (NeurIPS)*, 2019.
- [27] Z. Wang, A. C. Bovik, H. R. Sheikh, E. P. Simoncelli *et al.*, "Image quality assessment: from error visibility to structural similarity," *IEEE Transactions on Image Processing*, vol. 13, no. 4, pp. 600–612, 2004.
- [28] A. Geiger, P. Lenz, C. Stiller, and R. Urtasun, "Vision meets robotics: The KITTI dataset," *The International Journal of Robotics Research*, vol. 32, no. 11, pp. 1231–1237, 2013.
- [29] A. Kendall, M. Grimes, and R. Cipolla, "Posenet: A convolutional network for real-time 6-dof camera relocalization," in *Proceedings of the IEEE International Conference on Computer Vision*, 2015, pp. 2938–2946.
- [30] F. Xue, X. Wang, S. Li, Q. Wang, J. Wang, and H. Zha, "Beyond tracking: Selecting memory and refining poses for deep visual odometry," in *Proceedings of the IEEE Conference on Computer Vision and Pattern Recognition*, 2019, pp. 8575–8583.
- [31] A. CS Kumar, S. M. Bhandarkar, and M. Prasad, "Depthnet: A recurrent neural network architecture for monocular depth prediction," in *Proceedings of the IEEE Conference on Computer Vision and Pattern Recognition Workshops*, 2018, pp. 283–291.

- [32] R. Garg, V. K. BG, G. Carneiro, and I. Reid, "Unsupervised cnn for single view depth estimation: Geometry to the rescue," in *European Conference on Computer Vision*. Springer, 2016, pp. 740–756.
- [33] C. Godard, O. Mac Aodha, and G. J. Brostow, "Unsupervised monocular depth estimation with left-right consistency," in *Proceedings of the IEEE Conference on Computer Vision and Pattern Recognition*, 2017, pp. 270–279.
- [34] H. Zhan, R. Garg, C. Saroj Weerasekera, K. Li, H. Agarwal, and I. Reid, "Unsupervised learning of monocular depth estimation and visual odometry with deep feature reconstruction," in *Proceedings of the IEEE Conference on Computer Vision and Pattern Recognition*, 2018, pp. 340–349.
- [35] G. Wang, H. Wang, Y. Liu, and W. Chen, "Unsupervised Learning of Monocular Depth and Ego-Motion Using Multiple Masks," in *2019 International Conference on Robotics and Automation (ICRA)*. IEEE, 2019, pp. 4724–4730.
- [36] Y. Wang, P. Wang, Z. Yang, C. Luo, Y. Yang, and W. Xu, "Unos: Unified unsupervised optical-flow and stereo-depth estimation by watching videos," in *Proceedings of the IEEE Conference on Computer Vision and Pattern Recognition*, 2019, pp. 8071–8081.
- [37] Y. Zou, Z. Luo, and J.-B. Huang, "Df-Net: Unsupervised joint learning of depth and flow using cross-task consistency," in *Proceedings of the European Conference on Computer Vision (ECCV)*, 2018, pp. 36–53.
- [38] B.-U. Lee, H.-G. Jeon, S. Im, and I. S. Kweon, "Depth completion with deep geometry and context guidance," in *2019 International Conference on Robotics and Automation (ICRA)*. IEEE, 2019, pp. 3281–3287.
- [39] S. Imran, Y. Long, X. Liu, and D. Morris, "Depth coefficients for depth completion," in *2019 IEEE/CVF Conference on Computer Vision and Pattern Recognition (CVPR)*. IEEE, 2019, pp. 12 438–12 447.
- [40] C. Chen, S. Rosa, Y. Miao, C. X. Lu, W. Wu, A. Markham, and N. Trigoni, "Selective sensor fusion for neural visual-inertial odometry," in *Proceedings of the IEEE Conference on Computer Vision and Pattern Recognition*, 2019, pp. 10 542–10 551.
- [41] I. Goodfellow, J. Pouget-Abadie, M. Mirza, B. Xu, D. Warde-Farley, S. Ozair, A. Courville, and Y. Bengio, "Generative adversarial nets," in *Advances in Neural Information Processing Systems*, 2014, pp. 2672–2680.
- [42] C. Zhao, Y. Tang, and Q. Sun, "Deep direct visual odometry," *arXiv preprint arXiv:1912.05101*, 2019.
- [43] K. He, X. Zhang, S. Ren, and J. Sun, "Deep residual learning for image recognition," in *Proceedings of the IEEE Conference on Computer Vision and Pattern Recognition*, 2016, pp. 770–778.
- [44] A. E. Orhan and X. Pitkow, "Skip connections eliminate singularities," *arXiv preprint arXiv:1701.09175*, 2017.
- [45] N. Mayer, E. Ilg, P. Hausser, P. Fischer, D. Cremers, A. Dosovitskiy, and T. Brox, "A large dataset to train convolutional networks for disparity, optical flow, and scene flow estimation," in *Proceedings of the IEEE Conference on Computer Vision and Pattern Recognition*, 2016, pp. 4040–4048.
- [46] M. Abadi, A. Agarwal, P. Barham, E. Brevdo, Z. Chen, C. Citro, G. S. Corrado, A. Davis, J. Dean, M. Devin *et al.*, "Tensorflow: Large-scale machine learning on heterogeneous distributed systems," *arXiv preprint arXiv:1603.04467*, 2016.
- [47] D. P. Kingma and J. Ba, "Adam: A method for stochastic optimization," *arXiv preprint arXiv:1412.6980*, 2014.
- [48] Z. Yang, P. Wang, W. Xu, L. Zhao, and R. Nevatia, "Unsupervised learning of geometry with edge-aware depth-normal consistency," 2018.
- [49] R. Mahjourian, M. Wicke, and A. Angelova, "Unsupervised learning of depth and ego-motion from monocular video using 3d geometric constraints," in *Proceedings of the IEEE Conference on Computer Vision and Pattern Recognition*, 2018, pp. 5667–5675.
- [50] M. Grupp, "evo: Python package for the evaluation of odometry and SLAM." <https://github.com/MichaelGrupp/evo>, 2017.
- [51] R. Wang, S. M. Pizer, and J.-M. Frahm, "Recurrent neural network for (un-) supervised learning of monocular video visual odometry and depth," in *Proceedings of the IEEE Conference on Computer Vision and Pattern Recognition*, 2019, pp. 5555–5564.